PERGAMON

International Journal of Heat and Mass Transfer 46 (2003) 399–409

International Journal of HEAT and MASS TRANSFER

www.elsevier.com/locate/ijhmt

Heat transfer and bubble characteristics in a fluidized bed with immersed horizontal tube bundle

Sung Won Kim, Jung Yeul Ahn, Sang Done Kim *, Dong Hyun Lee

Department of Chemical and Biomolecular Engineering and Energy and Environment Research Center, Korea Advanced Institute of Science and Technology, DaeJeon 305-701, South Korea

Received 28 March 2002; received in revised form 26 July 2002

Abstract

The effect of gas velocity on the average and local heat transfer coefficients between a submerged horizontal tube (25.4 mm-OD) and a fluidized bed has been determined in a fluidized-bed-heat-exchanger ($0.34 \times 0.50 \times 0.6$ m-high) of silica sand particles. The heat transfer coefficients and the properties of bubble and emulsion phases were simultaneously measured at the same location around the tube circumference by thermocouples and an optical probe. The average heat transfer coefficient (h_{avg}) exhibits a maximum value with variation of gas velocity (U_g). The local heat transfer coefficient (h_i) exhibits maximum values at the side of the tube (0°). Bubble frequency (f_b) increases and the emulsion contacting time (t_e) decreases with increasing U_g. The h_i increases with increasing f_b and decreasing t_e. The f_b exhibits higher values and t_e is shorter at the bottom (under each side) than those at the top section of the tube. The t_e and bubble fraction (δ_b) have been correlated with Froude number. The predicted h_{avg} values of small particles based on the packet renewal model and the emulsion contacting characteristics around the tube well accord to the experimental data.

Keywords: Fluidized bed heat exchanger; Heat transfer; Horizontal tube; Bubble property; Optical fiber probe

1. Introduction

Fluidized beds have been widely used in heat recovery processes because of their unique ability of rapid heat transfer and uniform temperature. Fluidized bed heat exchangers (FBHEs) are employed to enhance heat transfer capacity in atmospheric and pressurized circulating fluidized bed boilers [1]. Heat transfer from hot solids to the heat exchanger surface in the bed is achieved by using in-bed tubes and/or water-walls. The bed-to-surface heat transfer coefficients are needed to design FBHE, where temperature control plays an important role.

Heat transfer between submerged surfaces and fine particles in fluidized beds is affected by local properties of emulsion and bubble phases that contact the heat exchanger surface, so that these properties are needed to determine the contact dynamics at the tube surface as input data to heat transfer models. Many investigators have examined the emulsion phase contact dynamics at the tube surface using temperature [2], pressure [3–5] measurements or capacitance probe method [6,7]. Although the correlations to predict the emulsion and bubble properties for heat transfer model of the vertical tube systems have been reported but the results of the horizontal tube system in gas-fluidized beds are relatively sparse in the literature.

In this study, the effect of gas velocity on the average and local heat transfer coefficients between a submerged horizontal tube and the fluidized bed has been determined in a FBHE of sand particles. The relationship between the bubble or emulsion properties and the heat transfer coefficients has been determined from thesimultaneous measurements using a heat transfer tube with an optical probe. The correlations of bubble

* Corresponding author. Tel.: +82-42-869-3913; fax: +82-42-869-3910.

E-mail address: kimsd@cais.kaist.ac.kr (S.D. Kim).

0017-9310/03/$ - see front matter
PII: S0017-9310(02)00296-X

Nomenclature

A	1–(projected area of tube/bed area) in Eq. (8)
A_{tube}	surface area of tube (m^2)
Ar	Archimedes number, $d_p^3\rho_g(\rho_s-\rho_g)g/\mu^2$
B_i	contacting time of individual bubble phase (s)
C_e	emulsion heat capacity (J/kg K)
C_{pg}	heat capacity of gas (J/kg K)
C_{ps}	heat capacity of solid particles (J/kg K)
D	tube diameter (m)
d_p	mean diameter of particle (m)
E_i	contacting time of emulsion phase (s)
f_b	bubble frequency (s^{-1})
f_e	emulsion phase frequency (s^{-1})
G	superficial mass fluidizing velocity (kg/m^2 s)
G_{mf}	minimum mass fluidizing velocity (kg/m^2 s)
g	acceleration due to gravity (ms^{-2})
h	heat transfer coefficient (W/m^2 K)
h_{avg}	average heat transfer coefficient (W/m^2 K)
h_{bottom}	heat transfer coefficient in tube bottom section (W/m^2 K)
h_g	heat transfer coefficient of bubble phase (W/m^2 K)
h_i	local heat transfer coefficient (W/m^2 K)
h_{max}	maximum heat transfer coefficient (W/m^2 K)
I	electric current (A)
k_e	thermal conductivity of emulsion phase (W/m K)
k_g	gas conductivity (W/m K)
k_s	thermal conductivity of solids particle (W/m K)
N	data number
Nu	Nusselt number, hd_p/k_g
Nu_T	Nusselt number based on tube diameter, hD/k_g
Nu_{top}	Nusselt number in tube top section, hd_p/k_g
P	center-to-center distance of adjacent tubes (m)
Pr	Prandtl number, $C_{pg}\mu/k_g$
Q	heat transfer rate (W/m^2)
Re	Reynolds number of particle, $U_g\rho_g d_p/\mu$
T_b	bed temperature (K)
T_s	temperature of tube surface (K)
t_b	root-square-average contacting time of bubble phase (s)
t_e	root-square-average contacting time of emulsion phase (s)
U_g	gas velocity (m/s)
U_{mf}	minimum fluidization velocity (m/s)
V	electric voltage (V)

Greek symbols

$\overline{\delta}_1$	absolute average percentage deviation
$\overline{\delta}_2$	root-mean-square percentage deviation
δ_b	bubble fraction
δ_e	emulsion phase fraction
ε_e	voidage of emulsion (packet)
ε_{mf}	voidage at minimum fluidizing state
ϕ_b	equivalent thickness of gas film around the contact points between particles
ϕ_s	shape factor of particle
ρ_e	emulsion (packet) density (kg/m^3)
ρ_g	gas density (kg/m^3)
ρ_p	apparent density of solid particle (kg/m^3)

fraction and the emulsion contacting time are proposed for the heat transfer model application. A model is proposed to predict the average heat transfer coefficients in the bed of small particles with variations of gas velocity and the particle properties based on the packet renewal model and the emulsion contacting characteristics around the tube.

2. Experimental

Experiments were carried out in a FBHE made of transparent acrylic plate ($0.34 \times 0.48 \times 0.60$ m high) as shown in Fig. 1. The wall of FBHE was designed to accommodate a steel tube bundle (each pipe: 0.34 m length $\times$ 25.4 mm OD). The tube bank and the position of the heat transfer probe is also shown in Fig. 1. The tube bank was designed in a triangular pitch

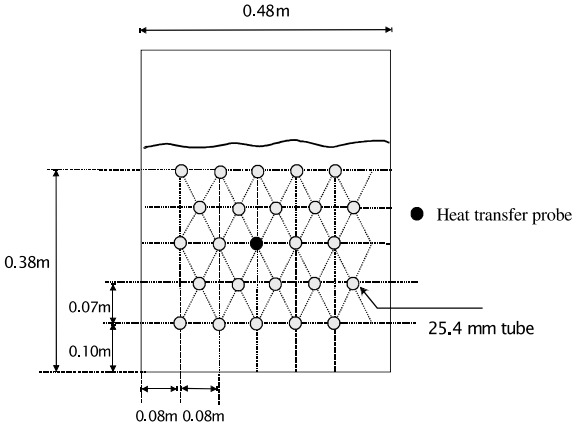

Fig. 1. Schematic diagram of the FBHE.

Table 1
Physical properties of particles in present and previous studies

Author	Tube diameter (mm)	Particles	d_p (μm)	ρ_s (kg/m^3)	U_{mf} (m/s)	C_{ps} (J/kg K)
This study	25	Sand	240	2582	0.048	710
Sunderesan and Clark [3]		Sand	317	2749	0.084	790
	50	Sand	483	2749	0.184	790
		Abrasive	535	2855	0.227	790
		Glass bead	467	2500	0.176	670
Doherty et al. [27]	28.6					
	50.8	Glass bead	270	2490	0.06	670
	76.2					
Grewal and Saxena [28]	12.7	Sand	167	2670	0.027	800
	28.6	Alumina	259	4015	0.104	766

(pitch length = 0.08 m) based on a previous study [8]. The first row was installed 0.10 m above the distributor plate accounting the jet length from the distributor. The solid particles used in this study were silica sand with a mean diameter of 240 μm and an apparent density of 2582 kg/m^3 that is similar to recycling ash in the FBHE operation [1] in a circulating fluidized bed (CFB). The properties of sand particles are listed in Table 1.

The schematic diagram of a heat transfer probe is shown in Fig. 2. The probe (25.4 mm OD) was made of a copper rod (80 mm-long) in which a 19.4 mm hole was drilled at the center of the rod to accommodate a

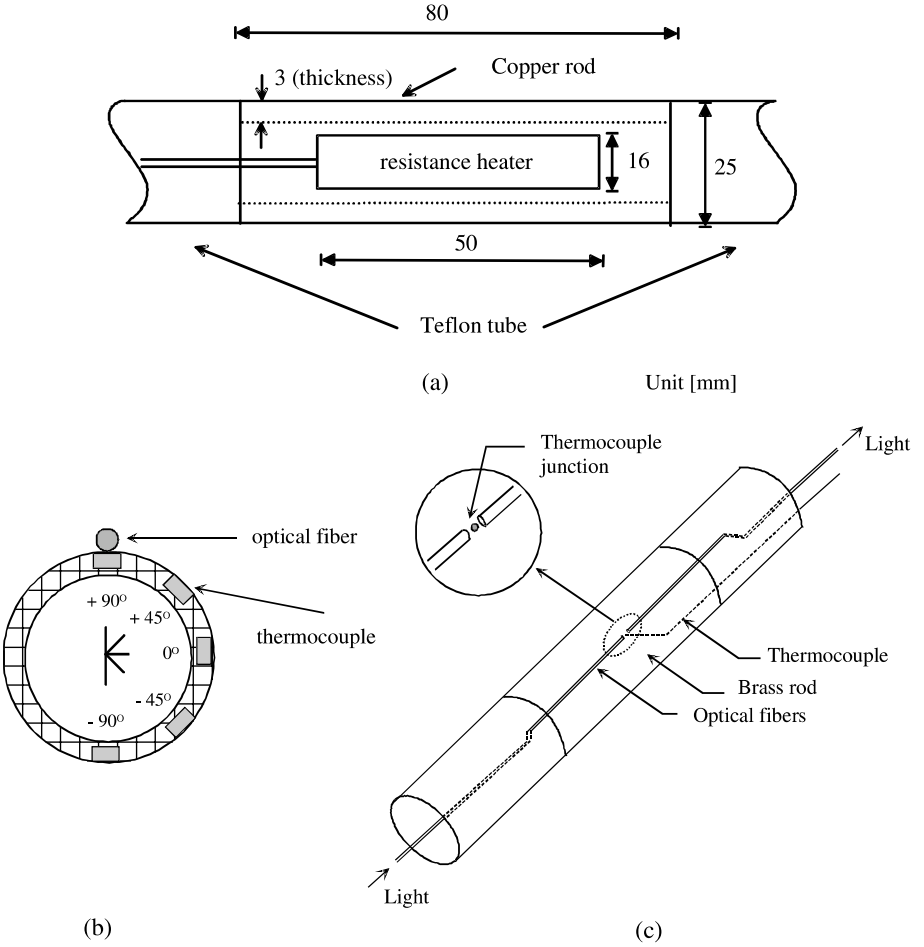

Fig. 2. Schematic diagram of the heat transfer probe (a) inside view, (b) cross sectional view, (c) measurement of bubble fraction.

resistance heater (16 mm-OD × 50 mm-long). At both sides of the probe, an 130 mm-long teflon support was installed to minimize the axial heat loss. A desired temperature of the copper rod or probe was controlled by a variable DC power supply. The supplied heat flux is determined by measuring voltage (V) and current (I) of the power supplier. Because temperature of the probe was higher than the bed temperature, heat was transferred from the probe to the bed, i.e. the opposite direction to that in a real FBHE. To measure the surface temperature of the probe tube, five thermocouples were installed around circumference of the probe tube at five different positions at an angle of 45 to one another as shown in Fig. 2(b). The thermocouples (fast response probe) are T-type with a bead of 0.13 mm-OD. The details of the thermocouple installation on the probe tube surface can be found elsewhere [4]. The heat transfer probe was located at the center of third row as shown in Fig. 1. The bubble properties were longitudinally uniform at the row as found in a previous study [9] at that location. Temperature signals from the thermocouple were amplified and sent via an A/D converter to a PC for recording. The sampling interval of signals was selected at 8 ms (125 Hz) [3] and signals were collected during the sampling time of 50 s for each experimental condition.

In this study, a transmission type of optical probe [10], which yields high signal-to-noise ratio with minimum disturbance in gas–solids flow compared to other methods [11], was used to detect the bubble and emulsion phase behavior simultaneously with the measurement of heat transfer coefficient. With the probe, only existence of bubble or emulsion phase can be detected. As shown in Fig. 2(c), an optical probe was constructed from two optical fibers (500 μm-OD), which were stuck to the tube surface in straight lines parallel to the tube axis. In the probe, one fiber was a light projector from a light source of a helium–neon laser (17 mW), and the other opposite site was a receiver of the transmitted light during bubbles passed the probe tips. The receiver was connected to a phototransistor, an amplifier, an A/D converter and PC. The sampling interval of signals was selected at 2 ms (500 Hz) and signals were collected during the sampling time of 28 s. Temperature signals were simultaneously collected with the same frequency of the optical signals at the same point. The heat transfer probe was allowed to rotate to change angle of the measuring position. The superficial air velocity (U_g) was varied in the range of 0–0.20 m/s. The bed height was kept at 0.37 m for all the experimental conditions.

3. Data analysis

The local heat transfer coefficient (h_i) can be determined from the known power input [voltage (V) × current (I)], surface area (A_{tube}) of the heat transfer tube and the measured temperatures of tube surface (T_s) and the bed (T_b) as

$$h_i = \frac{Q}{A_{tube}(T_s - T_b)} = \frac{IV}{A_{tube}(T_s - T_b)} \tag{1}$$

The average heat transfer coefficient for the whole tube (h_{avg}) is calculated by

$$h_{avg} = \frac{h_{+90^\circ} + 2h_{+45^\circ} + 2h_{0^\circ} + 2h_{-45^\circ} + h_{-90^\circ}}{8} \tag{2}$$

The signals from the optical fiber probe can be separated into bubble or emulsion phase based on the reference values [12]. With the contacting time of bubble (B_i) and emulsion phases (E_i), the root-square-average bubble and emulsion phase contacting time can be calculated from the following relations [2,6]

$$t_b = \left[\frac{\sum_i B_i}{\sum_i B_i^{1/2}}\right]^2 \text{ and } t_e = \left[\frac{\sum_i E_i}{\sum_i E_i^{1/2}}\right]^2 \tag{3}$$

The t_e is required as an input data to the heat transfer model based on the packet model to predict h_i [6].

The bubble and emulsion phase fractions are given by

$$\delta_b = \frac{\sum_{i=1}^{n} B_i}{\text{total sampling time}} \text{ and } \delta_e = \frac{\sum_{i=1}^{n} E_i}{\text{total sampling time}} \tag{4}$$

The bubble or emulsion phase frequency is determined by the number of each phase per unit time at the probe tip as

$$f_b \text{ or } f_e = \frac{\text{number of bubble or emulsion}}{\text{total sampling time}} \tag{5}$$

4. Results and discussion

4.1. Bubble and heat transfer characteristics at the tube surface

The effect of gas velocity on the average heat transfer coefficient (h_{avg}) is shown in Fig. 3. As can be seen, h_{avg} exhibits a maximum value (394 W/m^2 K) at U_g of 0.13 m/s (2.7 U_{mf}). The qualitative dependence of h_{avg} on U_g is in agreement with the reported values in previous studies [3,13]. To predict the maximum bed-to-surface heat transfer coefficient (h_{max}), Zabrodsky [14] proposed a dimensional correlation for Geldart's group B particles as

$$h_{max} = 35.8\rho_p^{0.2} k_g^{0.6} d_p^{-0.36} \tag{6}$$

As can be seen in Fig. 3, his correlation predicts well the obtained value of h_{max} in this study. The h_{avg} at U_g below

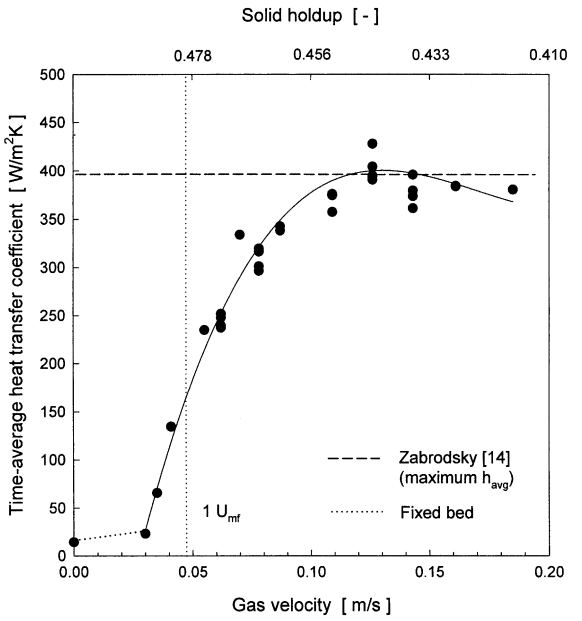

Fig. 3. Effect of gas velocity on the average heat transfer coefficient.

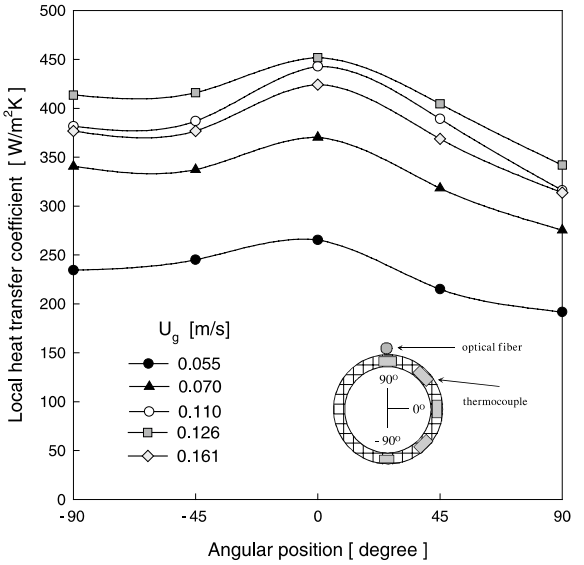

Fig. 4. The local time-averaged heat transfer coefficient for all angular positions at different gas velocity.

minimum fluidization velocity (U_{mf}) exhibits somewhat higher values than h_{avg} in a packed bed due to local fluidization. Local bubbles are observed due to the local increase of U_g between the tubes at U_g below U_{mf}, so that the bubble motion enhances h_{avg}.

The local time-averaged heat transfer coefficients (h_i) at all the angular positions with variation of U_g are shown in Fig. 4. The h_i exhibit their maximum value at the side (0°) of the tube. With increasing U_g, h_i increases due to increasing replacement of packets of particles at the tube surface. The h_i exhibits higher values at the lower than higher positions of the tube. An increase in U_g produces a greater effect on h_i for the top and bottom portions of the tube [3] as observed by Khan and Turton [15] in the high temperature beds. Around the tube surface, three different particle motions can be identified [2,3] as: (1) stationary with no particle movement at low U_g, (2) sliding of particles along the surface (3) mixing of emulsion and bubble phases. The maximum values of the heat transfer coefficient are observed at the boundary between sliding and mixing motions of particles [2]. Particle motions adjacent to a tube have a direct relation with bubble motion that may affect heat transfer in the bed. Therefore, it is important to understand the relationship between the heat transfer and bubble characteristics.

The local instantaneous surface temperatures and signals from the optical probe measured simultaneously at five different locations around the tube at $U_g = 0.13$ m/s are shown in Fig. 5. The peaks in signals from the optical probe indicate the presence of bubbles [10]. In the bottom regions (0°, −45°, −90°) of the tube, the peaks by bubbles correspond well to the variations of instantaneous temperature as reported in a previous study [16]. It means that the bed-to-surface heat transfer can be directly related to the particle motion induced by bubbles. The variation of temperatures at the +45° location is affected by bubble motion, together with sliding motion of solids to 0° location of the tube as reported in previous studies [2,3]. At the top of the tube (+90°), the variation of surface temperature with time is minimal compared to the other locations since we can see that only one bubble was detected in the given time interval with variation of bed temperature. If the heat transfer mechanism is governed by the particle packet movement, fluctuation of the heat transfer coefficient on the top of the tube may be small since solid particles or packets are less influenced by bubbles. However, the particles on the top of the tube could be replaced by fresh particles due to the movement of nearby passing bubbles or due to the downward sliding of unstable stagnant particles on top of the tube.

The local time-averaged heat transfer coefficient, bubble frequency and fraction of bubble or emulsion phase at different angular positions of the tube are shown in Fig. 6. The emulsion fraction is low at the bottom region of the tube and increases with increasing the angular position. The heat transfer rate between a tube and a fluidized bed depends on the particle concentration close to the heat transfer surface and particle residence time at the tube surface [13]. The larger values of h_i could be obtained with shorter residence time of

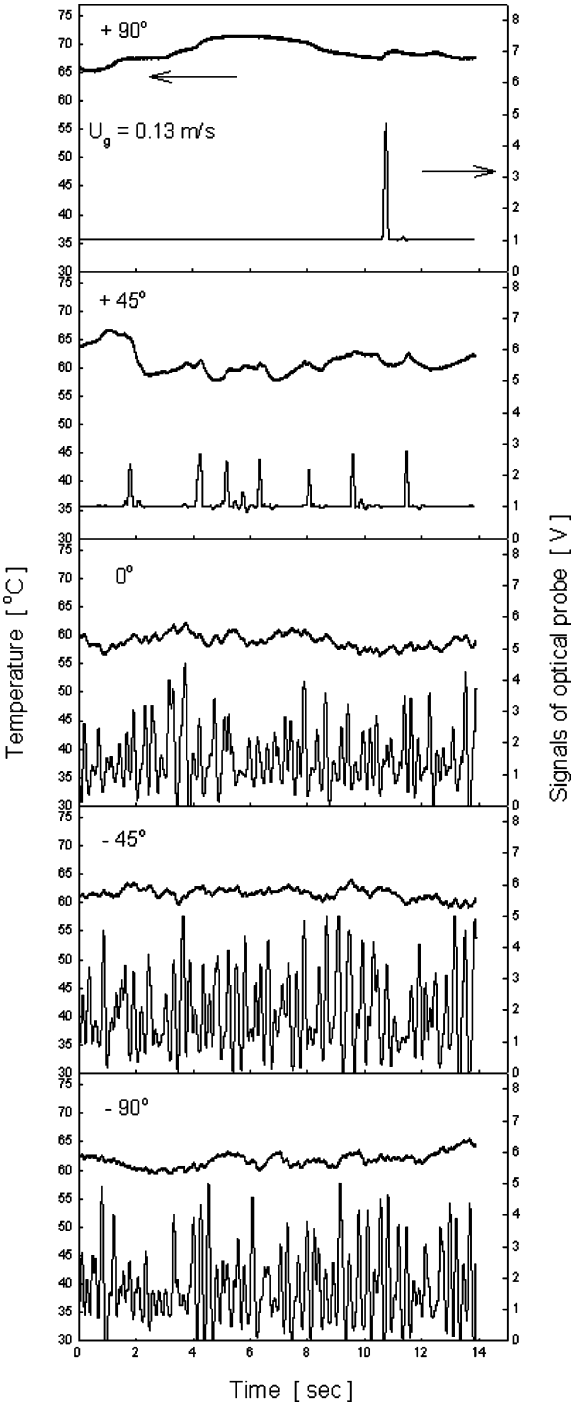

Fig. 5. Local instantaneous surface temperatures and optical probe signals measured simultaneously at the different angular locations around a tube ($U_g = 0.13$ m/s).

particles or packets with higher solid holdups. The particle residence time on the tube surface depends on the replacement rate of solid packets by bubbles. In the top region of the tube, h_i exhibits low value since solid particles reside longer on top of the tube with lower bubble frequencies. In the bottom region of the tube, h_i exhibits higher values due to short residence time with vigorous bubbling having high frequency in spite of lower emulsion fraction or solids holdups. Specially, h_i at side of the tube exhibits a maximum value due to short residence time of emulsion phase by bubbles rising from the tube bottom and sliding of particles from top section of the tube, which may produce more vigorous solids mixing having comparatively higher solids holdups [2].

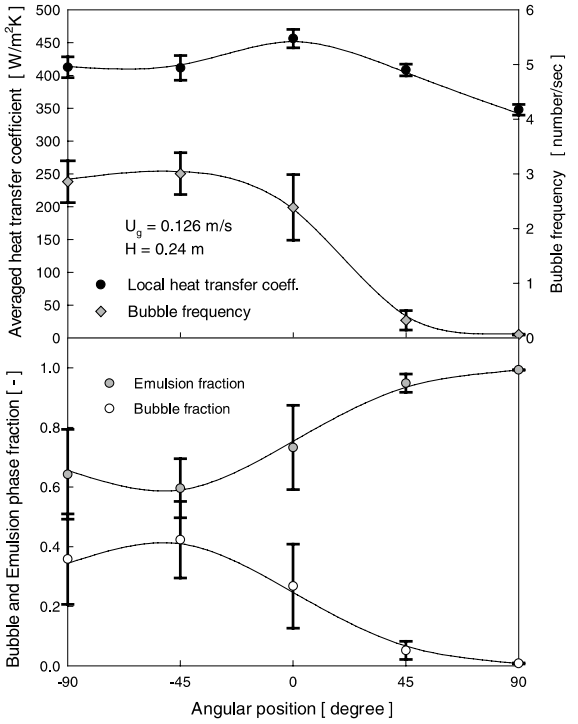

Fig. 6. The local time-averaged heat transfer coefficient, bubble frequency and bubble or emulsion phase fraction at all angular positions.

The effect of gas velocity on bubble frequency (f_b) at the different angular positions is shown in Fig. 7(a) where f_b increases with increasing U_g. As expected, f_b at the bottom region (under 0°) is higher than that at top region of the tube. As U_g is increased, bubbles are observed at top region of the tube (+45° location). A large distorted bubble passes without splitting between two tubes at higher gas velocities [9]. The contacting of the distorted bubble and solids sliding at that location lead to an increase in h_i (Fig. 4).

The relationship between f_b and the local heat transfer coefficient (h_i) is shown in Fig. 7(b). As can be seen, h_i increases with an increase in f_b that leads to increase in replacement rate of solid packets and solids mixing in the bed.

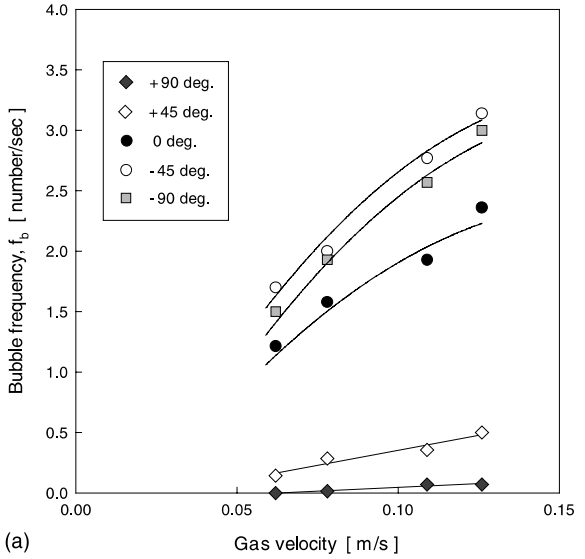

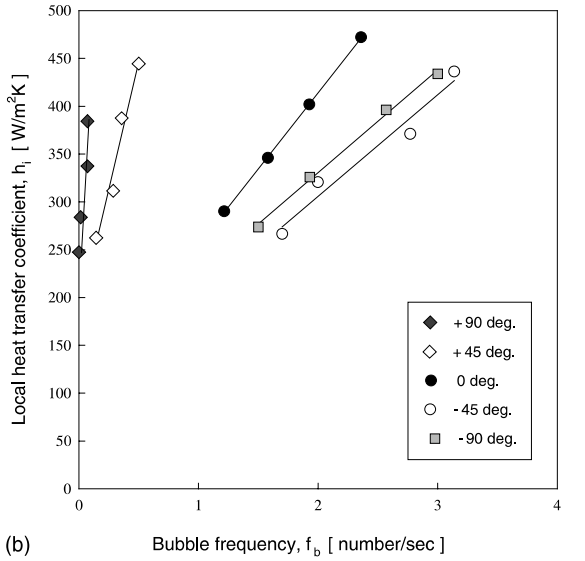

Fig. 7. (a) Effect of gas velocity on bubble frequency at different angular positions, (b) effect of bubble frequency on the local heat transfer coefficient.

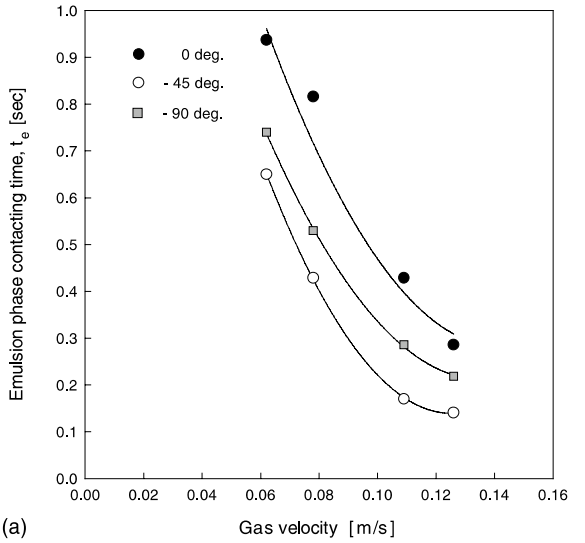

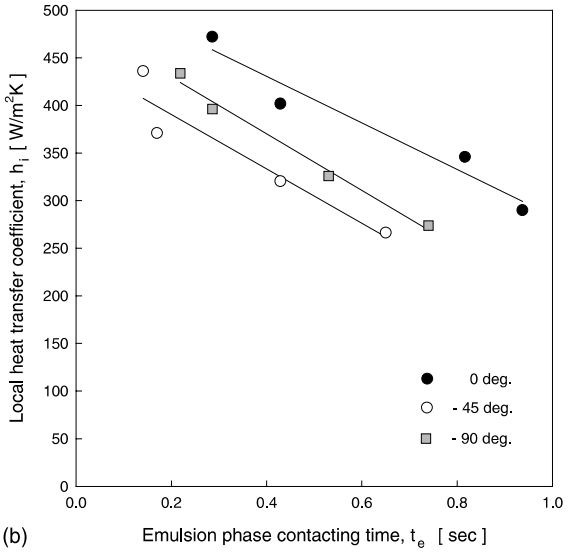

Fig. 8. (a) Effect of gas velocity on emulsion contacting time at tube bottom, (b) effect of emulsion contacting time on the local heat transfer coefficient.

The effect of U_g on emulsion contacting time (t_e) at bottom regions of the tube is shown in Fig. 8(a). As can be seen, t_e decreases with increasing U_g due to the increase of bubble frequency. Also, the relationship between t_e and h_i at bottom regions of the tube is shown in Fig. 8(b). As expected, h_i decreases with increasing t_e due to the reduced solids mixing [13]. At higher bubble frequencies, t_e would decrease, which provides higher surface renewal rate with higher solids mixing and consequent increase in h_i.

4.2. Prediction of heat transfer coefficient

Theoretical models have been proposed to estimate the heat transfer coefficient between the submerged tubes and fluidized beds [2,17–22]. One of the oldest and most widely accepted models is the packet renewal model [17,18]. In this model, as in many of the other models, residence time of the packets (emulsion) at the heat transfer surface is assumed to govern the heat transfer process. During the emulsion phase contact with the heat transfer surface, the heat transfer rate decreases with time due to the effect of the thermal

penetration depth, as in a semi-infinite solid. The model describes that the average heat transfer rate of the emulsion phase is dependent upon contact time of the emulsion phase.

The predicted time-averaged local heat transfer coefficient can be expressed as [17,18]:

$$h_i = (1-\delta_b)\frac{2}{\sqrt{\pi}}\sqrt{k_e\rho_e c_e}\frac{1}{\sqrt{t_e}} + \delta_b h_g \tag{7}$$

To determine h_i from Eq. (7), the values of bubble fraction (δ_b) and emulsion contact time (t_e) are needed [2,18,21]. The correlations to predict h_i in the bed of vertical tube system have been proposed [22], however, it is difficult to apply the correlations to the bed of horizontal tube system since bubble dynamics and heat transfer characteristics are affected by orientation of the tube surface in a fluidized bed [21]. Moreover, the correlations to predict δ_b and t_e are comparatively sparse in the beds of horizontal tube system.

The obtained δ_b values at the tube bottom region ($\leqslant 0°$) in present and previous studies [6,23,24] are correlated with Froude number based on the study of Baskakov et al. [22] as

$$\delta_b = 0.19\left[\frac{d_p g}{U_{mf}^2(U_g/U_{mf}-A)^2}\right]^{-0.23} \tag{8}$$

where $A = 1 -$ (projected tube area/bed area) that describes the local formation of bubbles between tubes at gas velocity below U_{mf}.

Comparison of δ_b values from Eq. (8) and the experimental data in the present and previous studies [6,23,24] is shown in Fig. 9 with the correlation of Baskakov et al. [22] for a vertical tube system.

Also, the obtained t_e values at bottom region ($\leqslant 0°$) of the tube in the present and previous studies [2,6] are correlated with Froude number [22] as

$$t_e = 1.20\left[\frac{d_p g}{U_{mf}^2(U_g/U_{mf}-A)^2}\right]^{0.30}\left(\frac{d_p}{D}\right)^{0.225} \tag{9}$$

Comparison between Eq. (9) and the measured t_e is shown in Fig. 10 with the correlation of Baskakov et al. [22] for vertical tubes and the data of previous studies [2,6].

To calculate h_i, the values of thermal conductivity, density and heat capacity of emulsion (packet) and the heat transfer coefficient of gas (h_g) are needed with the knowledge of δ_b and t_e.

The packet density can be calculated by

$$\rho_e = (1-\varepsilon_e)\rho_s \tag{10}$$

where ε_e is voidage of emulsion (packet) phase.

The correlation of ε_e in vicinity of the heat transfer tube in a fluidized bed is employed for considering the particle-tube contact geometry based on a previous study [21] as

$$\varepsilon_e = 1 - \frac{(1-\varepsilon_{mf})\left[0.7293 + 0.5139(d_p/D)\right]}{1+(d_p/D)} \tag{11}$$

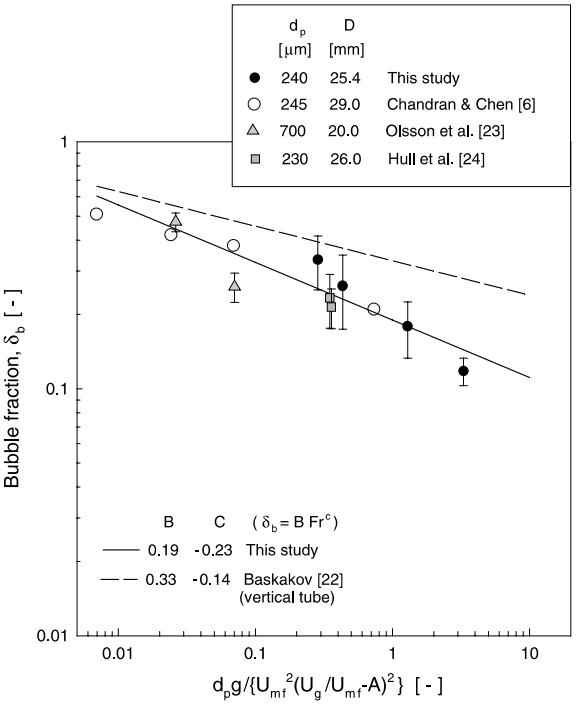

Fig. 9. Prediction of bubble fraction at the tube surface.

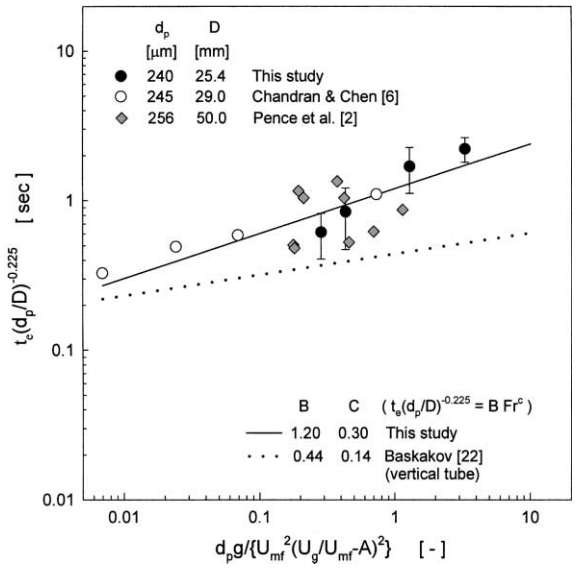

Fig. 10. Prediction of emulsion contacting time at the tube surface.

Since the fluidizing medium is gas, its heat capacity can be neglected relative to that of solids. The heat capacity of packets (C_e) is assumed to be equal to the heat capacity of solid (C_{ps}) [18]. In the theoretical calculation of the heat transfer coefficient in this study, the emulsion packet conductivity is taken as [25]

$$k_e = \varepsilon_e k_g + (1-\varepsilon_e)k_s\left[\frac{1}{\phi_b(k_s/k_g)+2/3}\right] \tag{12}$$

where ϕ_b is equivalent thickness of the gas film around the contact points between particles [25].

The h_g is obtained from the correlation of Baskakov et al. [22] as

$$h_g = 0.009\left(\frac{k_g}{d_p}\right)Ar^{0.5}Pr^{0.33} \tag{13}$$

The h_i can be calculated from Eqs. (8)–(13) in conjunction with Eq. (7).

The heat transfer coefficient depends on orientation of the heat transfer surface in fluidized beds [21,25]. As can be seen in Figs. 5–8, the emulsion contacting with the tube wall is different at top and bottom regions of the tube. This behavior around the tube has been substantiated by the measurement of local heat transfer coefficients [26]. Therefore, the packet model cannot be applied to the top section where direct bubble contacting is scarce compared to the bottom section of the tube. In this study, the top section regions (+45° and +90°) of the tube are assumed to be occupied by emulsion phase and the heat transfer in this region is governed by the movement of emulsion phase due to the movement of nearby bubbles. The h_{avg} values at the top sections of the tube in the present and previous [3] studies (Table 1) have been correlated with the dimensionless numbers based on previous studies [21,25] as

$$Nu_{top} = 47.56Re^{0.43}Pr^{0.33}(D/d_p)^{-0.74}(C_{ps}/C_{pg})^{-1.69} \tag{14}$$

with a correlation coefficient of 0.92 and a standard error of estimate of 0.70. The range of variables in Eq. (14) covers $0.97 \leqslant Re \leqslant 12.56$, $93.46 \leqslant D/d_p \leqslant 157.73$, $0.67 \leqslant C_{ps}/C_{pg} \leqslant 0.79$ and $Pr = 0.71$.

The calculated Nu_{top} values predict the experimental data of the present and previous [3] studies (Table 1) within ±20% as shown in Fig. 11.

Finally, Eq. (7) of the packet model is applied to the calculation of h_{avg} at the bottom section of the tube (0°, −45°, −90°), and Eq. (14) can be used for top section of the tube. The h_{avg} of the entire tube can be calculated by Eqs. (7) and (14) in conjunction with Eq. (2).

To estimate h_i with the immersed surface in a gas-fluidized bed, heat transfer behavior in the bed of small particles differs from that of larger ones in a qualitative sense due to the different predominant mechanism [21]. Therefore, in this study, the prediction of h_{avg} is limited to the smaller particles ($d_p \leqslant 535$ μm) that cover the ranges of correlations on f_b and t_e and the bed material in FBHE [2] for CFB application.

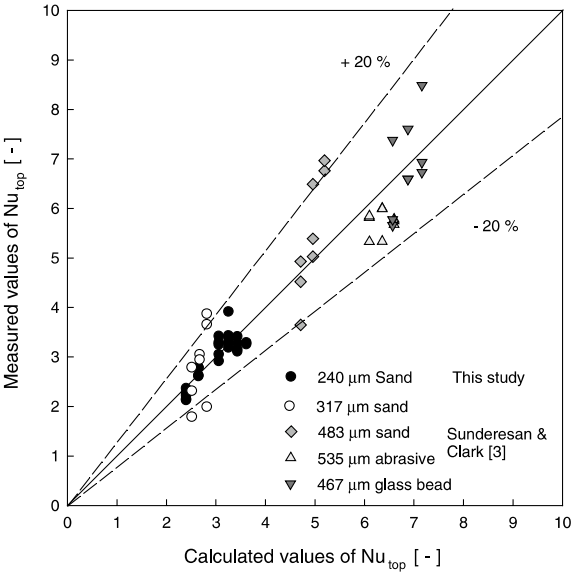

Fig. 11. Comparison of Nusselt number in tube top section obtained by the correlation and the experimental data.

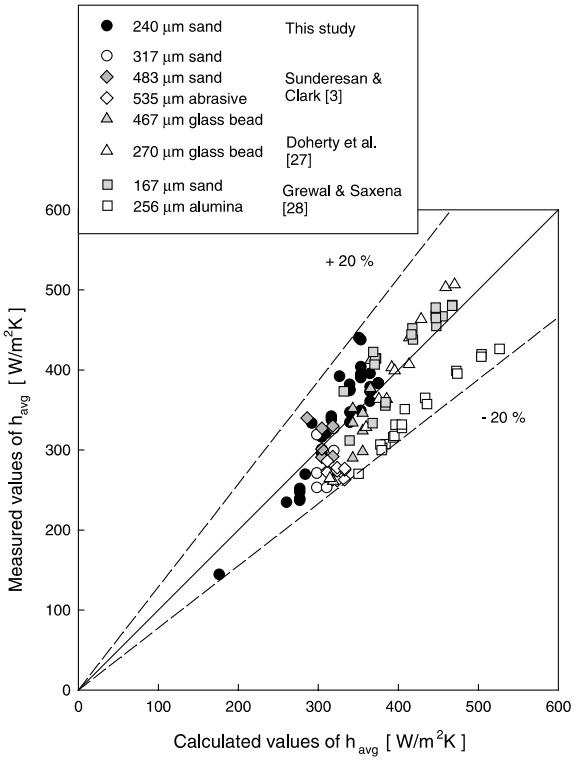

Fig. 12. Comparison of the average heat transfer coefficients obtained by the proposed model and the experimental data.

Table 2
Mean percentage deviation between predicted and experimental h_{avg}

Author	Correlations	$\overline{\delta}_1$	$\overline{\delta}_2$
Gelperin et al. [29]	$Nu_T = 4.38\left[\frac{1}{6(1-\varepsilon_e)}\left(\frac{Gd_p}{\mu}\right)\right]^{0.32}\left(\frac{1-\varepsilon_e}{\varepsilon_e}\right)\left(\frac{D}{d_p}\right)$	21.2	30.3
Petrie et al. [30]	$Nu_T = 14(G/G_{mf})^{1/3}Pr^{1/3}(D/d_p)^{2/3}$	33.8	43.2
Andeen and Glicksman [31]	$Nu_T = 900(1-\varepsilon_e)\left[\left(\frac{GD\rho_s}{\rho_g\mu}\right)\left(\frac{\mu^2}{d_p^3\rho_s^2 g}\right)\right]^{0.326}Pr^{0.3}$	39.7	45.3
Grewal [32]	$Nu_T = 47(1-\varepsilon_e)\left[\left(\frac{GD\rho_s}{\rho_g\mu}\right)\left(\frac{\mu^2}{d_p^3\rho_s^2 g}\right)\right]^{0.325}$ $\left(\frac{\rho_s C_{ps} D^{2/3} g^{1/2}}{k_g}\right)^{0.23} Pr^{0.3}\left(1-0.21(P/D)^{-1.75}\right)$ with $\varepsilon_e = \frac{1}{2.1}\left(0.4+\left(4\left(\frac{\mu G}{d_p^2(\rho_g(\rho_s-\rho_g))\phi_s^2 g}\right)^{0.43}\right)^{1/3}\right)$	25.7	31.3
This study	$h_{avg} = \frac{5}{8}h_{bottom} + \frac{3}{8}h_{top}$	11.2	13.6
	$h_{bottom} = (1-\delta_b)\frac{2}{\sqrt{\pi}}\sqrt{k_e\rho_e c_e}\frac{1}{\sqrt{t_e}} + \delta_b h_g$		
	$Nu_{top} = 47.56Re^{0.43}Pr^{0.33}(D/d_p)^{-0.74}(C_{ps}/C_{pg})^{-1.69}$		

$\overline{\delta}_1 = \frac{100}{N}\sum_{i=1}^{N}\left|\frac{\text{prediction}-\text{experimental}}{\text{experimental}}\right|$; $\overline{\delta}_2 = 100\sqrt{\frac{1}{N}\sum_{i=1}^{N}\left(\frac{\text{prediction}-\text{experimental}}{\text{experimental}}\right)^2}$.

The h_{avg} values measured in the present and previous studies [3,28,29] are compared with the calculated values from Eq. (2) as shown in Fig. 12. As can be seen, the calculated h_{avg} values predict the experimental data of the present and previous studies [3,27,28] within ±20% (Table 1).

A comparison between the calculated values of h_{avg} from the correlations in the literature [29–32] and the experimental values from the present and previous studies [3,27,28] is shown in Table 2. As can be seen, the present model based on the packet renewal model and the solids behavior around the tube predicts the h_{avg} values most accurately compared with the values from the reported correlations [29–32].

5. Conclusions

The effect of gas velocity on the average and local heat transfer coefficients between a submerged horizontal tube and the fluidized bed has been determined in a FBHE. The average heat transfer coefficient increases with increasing gas velocity toward a maximum value of the coefficient. The local heat transfer coefficient exhibits a maximum value at the side of the tube. The bubble frequency increases and the emulsion contacting time decreases with increasing gas velocity. The bubble fraction exhibits higher values and the emulsion-contacting time is shorter at the bottom compared to the top section of the tube. The local heat transfer coefficient increases with an increase in bubble frequency and a decrease in the average contacting time of emulsion phase. The average contacting time of the emulsion phase and bubble fraction have been correlated with Froude number. The calculated average heat transfer coefficient in the bed of small particles from the proposed model based on the packet renewal model and the emulsion contacting characteristics around the tube accords well to the experimental data.

Acknowledgement

We acknowledge a grant-in-aid for research from the Ministry of Commerce, Industry and Energy, Korea.

References

[1] P. Basu, S.A. Fraser, in: Circulating Fluidized Bed Boilers: Design and Operations, Butterworth-Heinemann, USA, 1991, pp. 55–94.
[2] D.V. Pence, D.E. Beasley, R.S. Figiola, Heat transfer and surface renewal dynamics in gas-fluidized beds, Journal of Heat Transfer 116 (1994) 929–937.
[3] S.R. Sunderesan, N.N. Clark, Local Heat transfer coefficients on the circumference of a tube in a gas fluidized bed, International Journal of Multiphase Flow 21 (1995) 1003–1024.
[4] D. McKain, N.N. Clark, C. Atkinson, R. Turton, Correlating local tube surface heat transfer with bubble presence in a fluidized bed, Powder Technology 79 (1994) 69–79.
[5] A.I. Karamavruc, N.N. Clark, A fractal approach for interpretation of local instantaneous temperature signals

around a horizontal heat transfer tube in a bubbling fluidized bed, Powder Technology 90 (1997) 235–244.
[6] R. Chandran, J.C. Chen, Bed-surface contact dynamics for horizontal tubes in fluidized bed, AIChE Journal 28 (1982) 907–914.
[7] S. Biyikli, K. Tuzla, J.C. Chen, Particle contact dynamics on tubes in the freeboard region of fluidized beds, AIChE Journal 33 (1987) 1225–1227.
[8] O Sitnai, A.B. Whitehead, in: J.F. Davidson, D. Harrison, R. Clift (Eds.), Fluidization, second ed., Academic Press, London, 1985, pp. 473–493.
[9] J.Y. Ahn, Bubble characteristics in a fluidized bed heat exchanger; M.S. thesis, KAIST, DaeJeon, Korea, 2001.
[10] Y.T. Choi, S.D. Kim, Bubble characteristics in an internally circulating fluidized bed, Journal of Chemical Engineering Japan 24 (1991) 195–202.
[11] J. Werther, Measurement techniques in fluidized beds, Powder Technology 102 (1999) 15–36.
[12] S.W. Kim, W. Namkung, S.D. Kim, Solids behavior in freeboard of FCC regenerator, Journal of Chemical Engineering Japan 33 (2000) 78–85.
[13] N.S. Grewal, S.C. Saxena, Maximum heat transfer coefficient between a horizontal tube and a gas–solid fluidized bed, Industrial and Engineering Chemistry Process Design Development 20 (1981) 108–116.
[14] S.S. Zabrodsky, Hydrodynamics and heat transfer in fluidized beds, MIT Press, Cambridge, MA, 1963.
[15] T. Khan, R. Turton, The measurement of instantaneous heat transfer coefficients around the circumference of a tube immersed in a high temperature fluidized bed, International Journal of Heat and Mass Transfer 35 (1992) 3397–3406.
[16] J. Baeyens, W.R.A. Goossens, Some aspects of heat transfer between a vertical wall and a gas fluidized bed, Powder Technology 8 (1973) 91–96.
[17] H.S. Mickley, D.F. Fairbanks, Mechanism of heat transfer to fluidized beds, AIChE Journal 1 (1955) 374–384.
[18] T.F. Ozkaynak, J.C. Chen, Emulsion phase residence time and its use in heat transfer models in fluidized beds, AIChE Journal 26 (1980) 544–550.
[19] N.I. Gel'perin, V.G. Ainshtein, L.A. Korotyanskaya, Heat transfer between a fluidized bed and staggered bundles of horizontal tubes, International Chemical Engineering 9 (1969) 137–142.
[20] J.S.M. Botterill, Gas Fluidization Technology, in: D. Geldart, John Wiley and Sons, UK, 1986, pp. 219–258.
[21] S.C. Saxena, Heat transfer between immersed surfaces and gas-fluidized beds, Advances in Heat Transfer 19 (1989) 97–190.
[22] A.P. Baskakov, B.V. Berg, O.K. Vitt, N.F. Fillippovsky, V.A. Kirakosyan, J.M. Goldohin, R.S. Figiola, Heat transfer to objects immersed in fluidized bed, Powder Technology 8 (1973) 273–282.
[23] S.E. Olsson, J. Wiman, A.E. Almstedt, Hydrodynamics of a pressurized fluidized bed with horizontal tubes: influence of pressure fluidization velocity and tube bank geometry, Chemical Engineering Science 50 (1995) 581–592.
[24] A.S. Hull, Z. Chen, J.W. Fritz, P.K. Agarwal, Influence of horizontal tube banks on the behavior of bubbling fluidized beds: 1. Bubble hydrodynamics, Powder Technology 103 (1999) 230–242.
[25] D. Kunii, O. Levenspiel, Fluidization Engineering, Butterworth-Heinemann, USA, 1991, pp. 313–336.
[26] J.S.M. Botterill, Fluid-Bed Heat Transfer, Academic Press, London, 1975, pp. 145–277.
[27] J.A. Doherty, R.S. Verma, S. Shrivastava, S.C. Saxena, Heat transfer from immersed horizontal tubes of different diameter in a gas-fluidized bed, Energy 11 (1986) 773–783.
[28] N.S. Grewal, S.C. Saxena, Experimental studies of heat transfer between a bundle of horizontal tubes and a gas–solid fluidized bed of small particles, Industrial and Engineering Chemistry Process Design Development 22 (1983) 367–376.
[29] N.I. Gel'perin, V.Y. Kruglikov, V.G. Ainshtein, Heat transfer between a fluidized bed and a surface, International Chemical Engineering 6 (1966) 67–73.
[30] J.C. Petrie, W.A. Freeby, J.A. Buckham, In-bed heat exchanger, Chemical Engineering Progress Symposium Series 64 (1968) 45–51.
[31] B.R. Andeen, L.R. Glicksman, Heat transfer to horizontal tubes in shallow fluidized beds, Proceedings of ASME-AIChE Heat Transfer Conference, St. Luouis, MO, 1976, Paper No. 76-HT-67.
[32] N.S. Grewal, A generalized correlation for heat transfer between a gas–solid fluidized bed of small particles and an immersed staggered array of horizontal tubes, Powder Technology 30 (1981) 145–154.